



Experimental Study on Heat Transfer Enhancement by Using Textile Flap Oscillation

Beihan Zhao, Wenshuo Yang, Chaolun Zheng, Yong Pei, Anthony Malatesta, Xinan Liu, and Bao Yang Department of Mechanical Engineering, University of Maryland, College Park, Maryland, USA

ABSTRACT

This paper experimentally studies a new method to enhance heat transfer in which a soft textile flap flutters and slaps a hot plate surface, due to fluid-structure interaction. The self-sustained periodic slapping of the textile flap against the heat transfer surface disrupts the boundary layers and thus, increases the heat transfer between the air and plate surface. Heat transfer coefficients in the presence of textile flaps of different shapes and sizes were measured while oscillatory motion of the flaps was recorded. The results show that rectangular flaps provide consistent heat transfer enhancement with increases in heat transfer coefficient observed of up to 42%, from 113 W·m⁻²·K⁻¹ in the absence of a textile flap, to 161 W·m⁻²·K⁻¹ in the presence of a rectangular textile flap, at a wind speed of 18.5 m·s⁻¹. It is found that the Nusselt number in the presence of rectangular flaps varies with the flap oscillation frequency in a nonlinear fashion and that the maximum heat transfer coefficient generally occurs when the dimensionless flow-induced oscillation frequency is in the range of 0.22 to 0.32. These results show the potential of using self-sustained oscillating textile flaps to enhance the convective heat transfer in various heat exchangers.

Introduction

Efficient convective heat transfer is essential in many engineering applications, such as heat exchangers, electrical devices, and power generation systems and many techniques have been investigated to increase rates of heat transfer [1–8]. Among the approaches studied, the use of active or passive vortex generators placed upstream of heat transfer surfaces to disrupt boundary layers has been extensively investigated [1, 9–12].

Active vortex generators use external power sources, such as piezoelectrics, to drive and control vortex flows [13–18]. Gerty [13] embedded a piezoelectric reed inside a heated duct which oscillates and induces a reverse Karman vortex street through the channel, leading to a nearly 100% increase of the Nusselt number (Nu). Hidalgo et al. [14] studied the heat transfer and fluid mechanics associated with the vibration of a piezoelectric reed in a 2.5 mm \times 27.4 mm channel demonstrating an increase in the heat transfer coefficient by a factor of up to 1.4. Acikalin et al. [16, 17] investigated the effects of piezoelectric fans on the thermal management of electronic devices showing a localized 100% increase of the convective heat transfer coefficient. Though actively controlled vortex generators have

shown promising results regarding heat transfer enhancement, practical implementation presents integration challenges due to increased system complexity as well as size, weight, and power concerns depending on the application.

Passive vortex generators, on the other hand, can modify the flow in the wake without requiring external power sources. Both rigid and flexible passive vortex generators have been explored to enhance heat transfer [9, 10, 19-27]. Wang et al. [10] carried out a comparative study of the air-side heat transfer of finand-tube heat exchangers in the presence of plain, louver, and semi-dimple rigid vortex generators. They found that the heat transfer coefficient increased by about 20% when louver rigid vortex generators were used. Li et al. [19] studied the air-side heat transfer of rectangular heatsink channels in the presence of an airfoil-shaped flexible vortex generator reporting improved heat transfer of 26%. Inspired by the caudal fin of fish, Li et al. [20] further investigated the heat transfer performance of an hourglass-shaped selfoscillating flexible vortex generator installed inside a plate-fin heat exchanger. A 68% enhancement in thermal-hydraulic characteristics was achieved when

Nomenclature			
A	total area of the hot plate for convective heat transfer, m ²	T_{back}	temperature on the back surface of the insulation layer, K
A_{c} A^{*} c_{p} D_{H} f f_{D} C^{*}	cross section area, m ² area ratio of the flexible structure to the total heat transfer area specific heat of the air, kJ·kg ⁻¹ ·K ⁻¹ hydraulic diameter for vertical wind tunnel, m oscillating frequency of the flexible textile flap, Hz Darcy friction factor	$T_{ m inlet}$ $T_{ m surface}$ $T_{ m air}$ U V W	inlet air temperature, K temperature of the hot plate surface, K averaged airflow temperature, K inlet air velocity, m/s input voltage, V Widths of the rectangular oscillating structures, m
$f^* \\ h \\ H \\ k \\ k_{\rm foam} \\ K \\ L \\ L_{\rm foam} \\ L_{HP} \\ Nu \\ p \\ P_{\rm atm} \\ p \\ P_{\rm o} \\ Pr \\ Pr_{\rm w} \\ Q_{\rm input} \\ Q_{\rm loss} \\ R \\ R_{\rm g} \\ Re \\ t$	dimensionless flow-induced oscillation frequency heat transfer coefficient, $W \cdot m^{-2} \cdot K^{-1}$ height difference of two water columns, mm thermal conductivity of air, $W \cdot m^{-1} \cdot K^{-1}$ thermal conductivity of the insulation foam, $W \cdot m^{-1} \cdot K^{-1}$ coefficient defined as $K = \frac{Nu}{Re-1000}$ lengths of the rectangular oscillating structures, m thickness of the insulation foam, m hot plate length, m Nusselt number static pressure, Pa atmosphere pressure, Pa perimeter of the cross section, m stagnation pressure, Pa Prandtl number Prandtl number of air at wall temperature power dissipation, W heat conduction loss, W resistance of the heater, Ω specific gas constant, $J \cdot kg^{-1} \cdot K^{-1}$ Reynolds number time, s	Subscripts atm back c D foam g H HP inlet input loss surface w	uncertainty specific weight of water, $kN \cdot m^{-3}$ dynamic viscosity of the air, $kg \cdot m^{-1} \cdot s^{-1}$ air density, $kg \cdot m^{-3}$
R R _g Re	resistance of the heater, Ω specific gas constant, $J \cdot kg^{-1} \cdot K^{-1}$ Reynolds number	surface	hot plate surface

compared to the clean channel at the same Reynolds number (Re). Ali et al. [23] conducted a numerical study on the effects of flexible flap oscillation on mixing and heat transfer in a two-dimensional flow. They predicted an increase of up to 97% in local heat transfer and 134% in overall heat transfer by using flexible instead of rigid flaps. Lee et al. [25, 26] numerically investigated the dynamics of a pair of flexible flags clamped in a heated channel finding that the presence of the flags with optimal parameters could increase the convective heat transfer by 207% and the thermal efficiency factor by 135% in comparison with the open channel flow.

As described in the literature, vortex generators are used to modify the flow in wake regions and enhance thermal mixing and heat transfer within the flow. In the present study, a new method is introduced to enhance the air-side heat transfer which takes advantage of fluid-structure interaction to produce a self-sustained fluttering of a soft textile flap placed on the top of a heated plate. The fluttering motion of the textile flap is achieved via the aerodynamic forces applied by the existing flow without requiring external energy

sources. The textile flap periodically slaps (i.e., directly contacts) the plate surface and disrupts the boundary layers, resulting in an enhancement in the heat transfer between the surface and the fluid.

The present experiments were designed and conducted to investigate the effects of the flow-induced oscillating-slapping motion of flexible flaps on the heat transfer performance of the plate. Heat transfer coefficients between the air and the heated plate in the presence of flexible textile flaps of different shapes and sizes were measured while the oscillatory motions of the textile flaps were captured with a high-speed camera. Using the experimental data, the relationship between the overall heat transfer performance and the oscillating dynamic features of the flexible textile flaps was explored with particular focus on oscillation frequency.

Experimental setup

Test apparatus

Figure 1 shows the schematic of the experimental setup for (a) heat transfer measurement and (b) dynamics observation of the textile flap. The experiments were

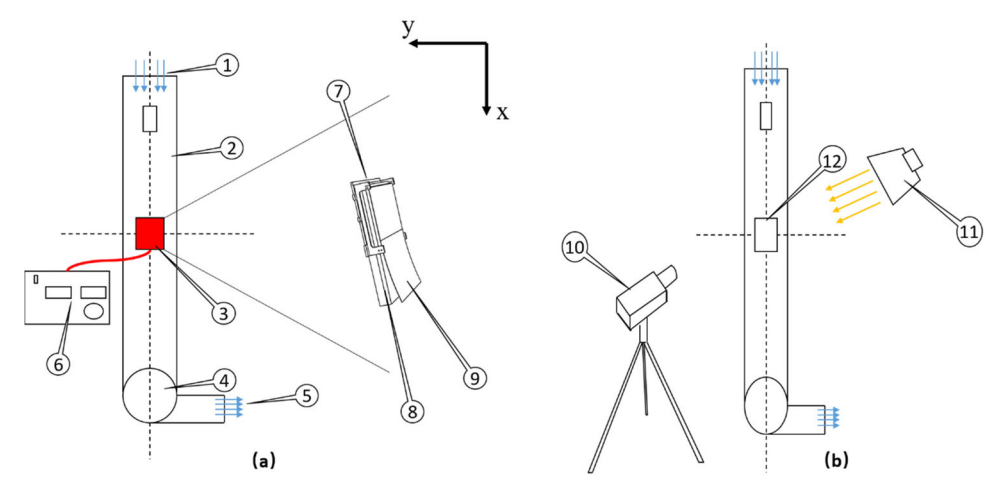


Figure 1. Schematic of the experimental setup for (a) heat transfer measurement and (b) dynamics observation of the textile flap. 1. air inlet; 2. vertical wind tunnel; 3. hot plate heat; 4. fan; 5. air outlet; 6. console and power supply; 7. 3D-printed supporting structure; 8. hot plate with thermal insulation foam; 9. flexible self-oscillating textile flap; 10. high-speed camera; 11. Halogen lamp; 12. observation window.

conducted in a cross-flow heat exchanger (H351, made by P. A. Hilton) in a vertical wind tunnel, as shown in Figure 1(a). The wind tunnel is 1 m in length and 0.15×0.05 m² in cross-section and downward airflow in the tunnel is driven by a variable-speed fan located at the bottom of the wind tunnel. The inlet air velocity (U) in the tunnel was measured at a distance of 0.13 m downstream from the inlet with a U-tube manometer, and was calculated using Bernoulli's equation in the form as

 $U = \sqrt{2(P_0 - p)/\rho}$, where P_0 is the stagnation pressure, p is the static pressure, and ρ is the air density. The difference between the stagnation pressure and static pressure was displayed by the height difference of the two water columns in the U-tube manometer. That is, $P_0 - p = \gamma_w H$, where $\gamma_w = 9.8 \text{ kN/m}^3$ is the specific weight of the water and H is the height difference of the two water columns. Thus, U can be expressed as $U = \sqrt{2\gamma_w H/\rho}$. The air density was calculated by using the ideal gas law as $\rho = p_{atm}/R_g T_{inlet}$, where p_{atm} is local atmospheric pressure measured in the lab, R_g = 287.06 J·kg⁻¹·K⁻¹ is the specific gas constant, and T_{inlet} is the inlet air absolute temperature in degrees Kelvin. In this study, the height differences of the water columns ranged from 6.0 to 21.0 mm, corresponding to a range of 9.9 to 18.5 m/s for the air velocity.

An aluminum hot plate was placed on the sidewall of the tunnel at a distance of 0.45 m from the entrance, as shown in Figure 1(a). An electric heater was embedded in the pre-drilled hole on one edge of the hot plate while a type K thermocouple was embedded in another pre-drilled hole on the opposite edge of the plate. A layer of thermal insulation foam was applied between the hot plate and tunnel sidewall to minimize the heat loss. During the experiments,

the power of the electric heater was set to a constant 70.45 W and steady state air temperatures just upstream and downstream of the hot plate were recorded for each test condition.

To visualize the oscillation of the textile flap, the hot plate was replaced with a transparent polymethyl methacrylate (also known as acrylic) plate with the same dimensions, as shown in Figure 1(b). A highspeed camera (V9, made by Vision Research Inc.) was used to observe the dynamic motion of the textile flap. Images were captured at 1000 frames per second with a resolution of 1632×1200 active pixels. Illumination for imaging was provided by a halogen lamp (part 11 in Figure 1(b)).

Figure 2 shows the schematic of the hot plate with the flexible textile flap which was made of commercial microfiber fabric (80% Polyester and 20% Polyamide, about 0.6 mm thick). While the bottom end of the textile flap was free to move, the top end of the textile flap was firmly attached to a stainless steel wire on a 3 D-printed frame structure placed on the hot plate base, as shown in Figure 2. The stainless steel wire was parallel to the hot plate surface and the distance between the wire and the plate surface was 3.78 mm. This distance is slightly larger than the thickness of thermal boundary layer at the edge of the flat plate, which is about 2.69 mm when the Reynolds number Re = 100,000. When the air flows over this assembly, a self-oscillation of the textile flap is generated.

Design of textile flaps

The geometry of the textile flaps was investigated in a two-step process, initially focusing on shape. Figure 3

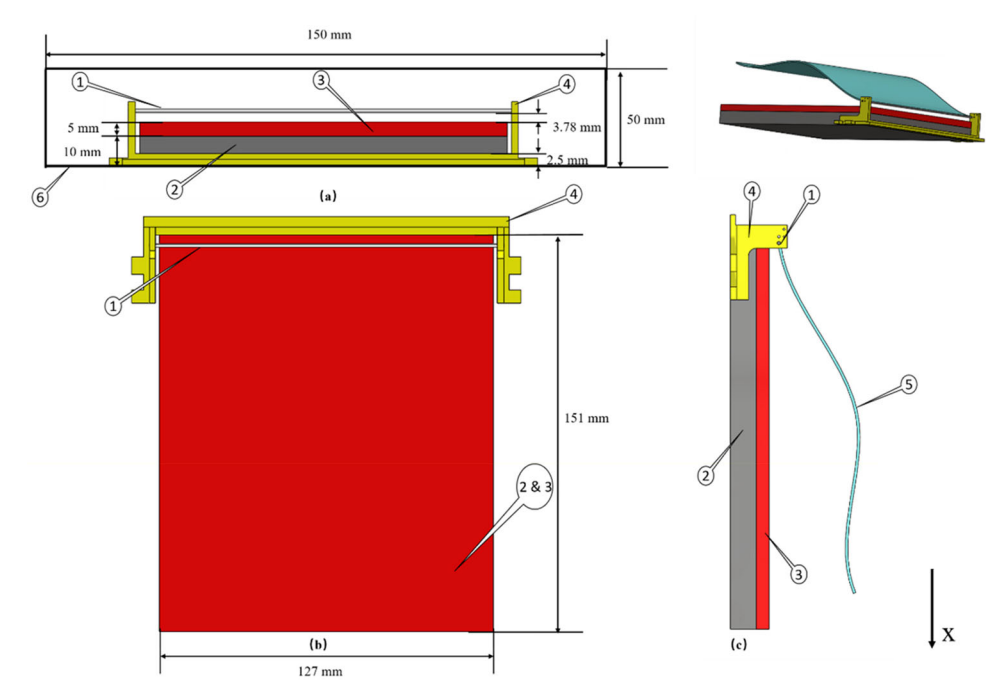


Figure 2. Schematic of the hot plate with the textile flap. (a) top view, (b) front view, (c) side view. 1). stainless steel wire; 2). thermal insulation foam; 3). hot plate; 4).3D printed supporting structure; 5). flexible textile flap; 6). wind tunnel cross-section; x = airflow direction

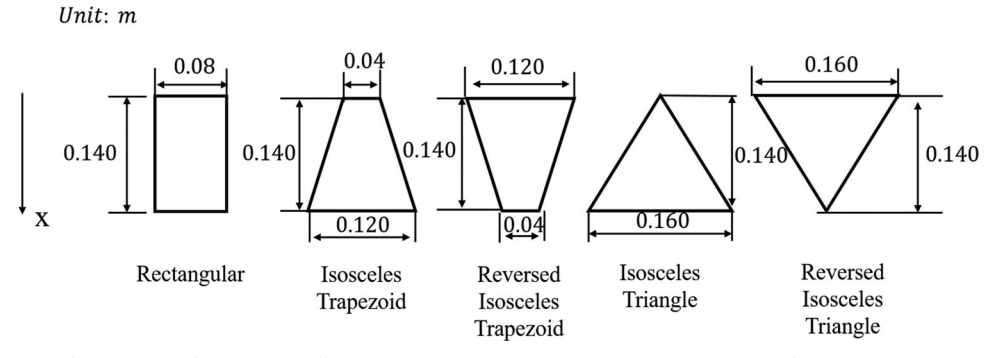


Figure 3. Schematic of the textile flaps with different shapes but the same area. x denotes airflow direction

shows five different shapes of flexible flaps used in the present study, all of which have an area of 0.0112 m². The goal of this part of the design was to determine the shape of textile flaps that can provide the most significant enhancement of heat transfer. Having found superior heat transfer performance from the rectangular textile flaps (see results below), twelve rectangular flaps with four different lengths and three different widths were then tested, as shown in Figure 4. The insert in the right of Figure 4 shows a sample textile flap marked with a pattern of two rows of dots on the mesh lines on the free end of the flap. This pattern was designed for measurement of the oscillatory motion of the textile flap within the flow.

Experimental uncertainty and validation of test apparatus

In the present study, the air-side heat transfer coefficient h is determined as follows:

$$h = \frac{Q_{\text{input}}}{A(T_{\text{surface}} - T_{\text{air}})} \tag{1}$$

where $Q_{\rm input}=V^2/R$ is the power of the electric heater, V is the input voltage, R is the resistance of the heater, $A=0.022~{\rm m}^2$ is the surface area of the hot plate, $T_{\rm surface}$ is the temperature at the hot plate surface, and $T_{\rm air}$ is the temperature averaged from the inlet and outlet airflows. The heat loss from the back of the hot plate $Q_{\rm loss}$ was estimated by Fourier's law as

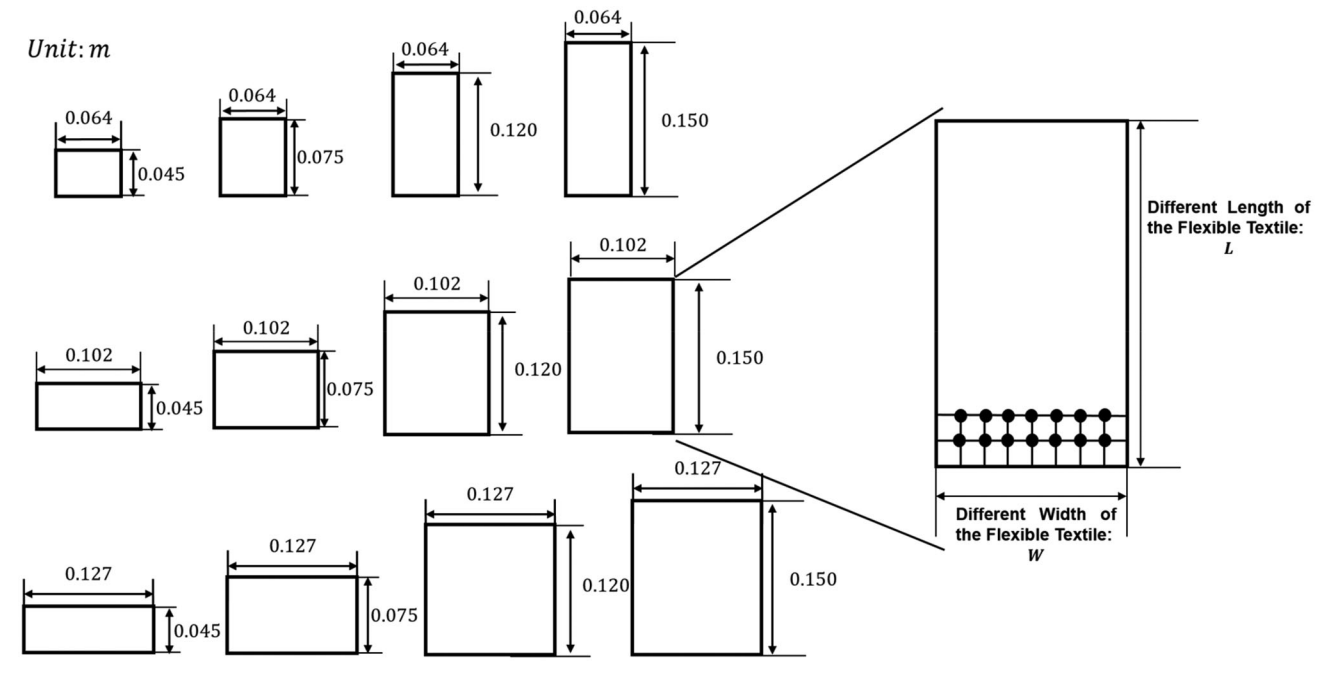


Figure 4. Schematic of the twelve rectangular textile flaps with different lengths and widths. Dots and meshes marked on the right textile flap are used for oscillation motion observations with the high-speed camera.

$$Q_{\rm loss} = k_{\rm foam} A \frac{T_{\rm surface} - T_{\rm back}}{L_{\rm foam}}$$
 (2)

where, $k_{\text{foam}} = 0.03 \text{ W} \cdot \text{m}^{-1} \cdot \text{K}^{-1}$ is the thermal conductivity of the insulation foam, $L_{\text{foam}} = 0.01 \text{ m}$ is the foam thickness and T_{back} is the temperature at the back surface of the insulation foam, which is approximately equal to the ambient temperature T_{amb} . With the temperature difference, $T_{\text{surface}} - T_{\text{back}}$, in the range of around 22 K to 50 K in this study, the magnitude of Q_{loss} is found to be in the range of 1.45 to 3.30 W, which is less than 5% of the power input 70.45 W. Thus, the heat loss is treated as negligible in the following calculations of the heat transfer coefficient.

The experimental uncertainty of the heat transfer coefficient (δh) in the present study is estimated by using the root-sum-square method [28] as

$$\delta h = \sqrt{\left(\frac{\partial h}{\partial Q}\delta Q\right)^2 + \left(\frac{\partial h}{\partial A}\delta A\right)^2 + \left(\frac{\partial h}{\partial T}\delta T\right)^2}$$
 (3)

where δQ , δA , and δT are the experimental uncertainties of the power of the electric heater, the surface area of the hot plate, and temperature, respectively. The relative uncertainties of the input voltage and the resistance of the heater are less than 0.1%, and thus δQ is negligible. The relative uncertainty of δA is less than 0.5% and can also be considered negligible. Thus, taking $\delta Q = 0$ and $\delta A = 0$, Eq. (3) reduces to

$$\frac{\delta h}{h} = \left| \frac{1}{T_{\text{surface}} - T_{\text{air}}} \right| \delta T \tag{4}$$

Substituting $\delta T = 1.1$ K for type K thermocouple and the range of $(T_{\text{surface}} - T_{\text{air}})$ which is from 22 K to 50 K used in the present study into Eq. (4) yields $\frac{\delta h}{h}$ < 10.0%.

The uncertainty of inlet air velocity (δU) can also be estimated by using the root-sum-square method

$$\delta U = \sqrt{\left(\frac{\partial U}{\partial H}\delta H\right)^2 + \left(\frac{\partial U}{\partial T_{\text{inlet}}}\delta T_{\text{inlet}}\right)^2 + \left(\frac{\partial U}{\partial p_{\text{atm}}}\delta p_{\text{atm}}\right)^2}$$
(5)

where δH , δT_{inlet} , and δp_{atm} are the uncertainties of the height difference of the two water columns, inlet air temperature, local atmosphere pressure, respectively. Dividing Eq. (5) with the expression of U yields

$$\frac{\delta U}{U} = \frac{1}{2} \sqrt{\left(\frac{\delta H}{H}\right)^2 + \left(\frac{\delta T_{\text{inlet}}}{T_{\text{inlet}}}\right)^2 + \left(\frac{\delta p_{\text{atm}}}{p_{\text{atm}}}\right)^2}$$
 (6)

in which δH is about 0.5 mm, δT_{inlet} is 1.1 K, and $\delta p_{\rm atm}/p_{\rm atm}$ is about 0.1% and can be considered negligible. Substituting the range of H and T_{inlet} (around 295.2 K) used in the present study into Eq. (6) yields $1.2\% < \frac{\delta U}{U} < 4.2\%$. The test apparatus is validated by the Gnielinski correlation [29, 30] in the absence of a textile flap. The Gnielinski correlation depicting the



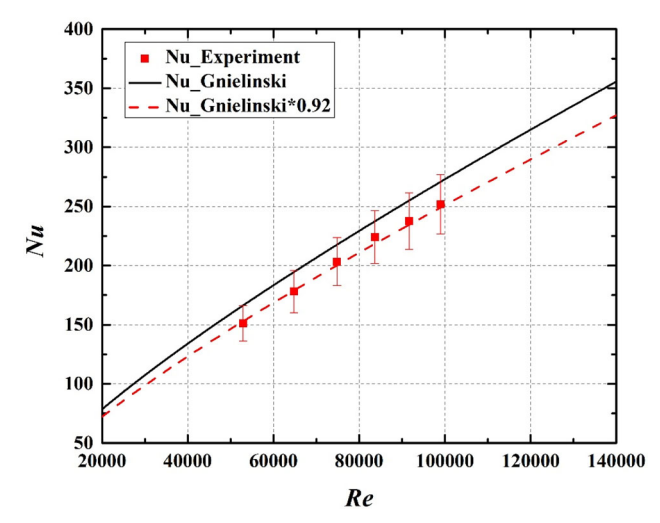


Figure 5. Comparison of the prediction with the Gnielinski correlation (solid line) [29, 30] and experimental measurement (squares) of Nusselt number Nu versus Reynolds number Re in the absence of a textile flap. The dash line refers to Nu that is 8% less than the prediction.

Nusselt number for internal turbulent channel flow is given as follows [29, 30],

$$Nu = \frac{\left(\frac{f_D}{8}\right)(Re - 1000)Pr}{1 + 12.7\sqrt{\frac{f_D}{8}\left((Pr)^{\frac{2}{3}} - 1\right)}} \left[1 + \left(\frac{D_H}{L}\right)^{2/3}\right] \left(\frac{Pr}{Pr_w}\right)^{0.11}$$

where f_D is the friction factor, $Nu=\frac{hD_{\rm H}}{k}$, $Re=\frac{\rho UD_H}{\mu}$ and $Pr=\frac{\mu c_p}{k}$ are the Nusselt number, Reynolds number and Prandtl number, respectively. Here, k is the thermal conductivity of air, μ is the dynamic viscosity of air, c_p is the specific heat of air, ρ is the air density, L is the length of the hot plate in the direction of wind propagation, and $D_{\rm H}=\frac{4A_c}{P}$ is the hydraulic diameter of the vertical wind tunnel, where $A_c =$ 0.15×0.05 m² is the cross section area and $P = 2 \times (0.15 + 0.05) = 0.4 \,\mathrm{m}$ is the perimeter of the cross section. $Pr_{\rm w}$ is the Prandtl number of air at wall temperature. The Gnielinski correlation for internal turbulent channel flow has errors of ±10%. In the present study, the air temperature ranges from 21 °C to 23 °C. For this small temperature range, ρ , k, μ , and c_p show little change and the values of these properties at 22 °C are used (i.e. $\rho = 1.2 \text{ kg} \cdot \text{m}^{-3}$, $k = 0.026 \text{ W} \cdot \text{m}^{-1} \cdot \text{K}^{-1}, \qquad \mu = 1.822 \times 10^{-5} \text{ kg} \cdot \text{m}^{-1} \cdot \text{s}^{-1},$ and $c_p = 1.007 \,\mathrm{kJ \cdot kg^{-1} \cdot K^{-1}}$. Thus, Pr = 0.705 is a constant and Re is in the range of $5.2 \times 10^4 - 9.9 \times$ 10^4 , while Eq. (7) is valid for 0.5 < Pr < 2000 and $3000 < Re < 5 \times 10^6$ [29, 30]. In the absence of a textile flap, the wind tunnel can be regarded as a smooth channel and f_D in Eq. (7) is estimated by using the Petukhov correlation [30],

$$f_D = (0.790 \ln Re - 1.64)^{-2}, \ 3000 \le Re \le 5 \times 10^6$$
 (8)

The correction term of $(\frac{p_r}{Pr_w})^{0.11}$ in Eq. (7) is approximated to be one due to the small exponential index and the moderate temperature change. Using the assumptions described above, Figure 5 shows the comparison of the prediction with Eq. (7) and experimental measurement of Nu versus Re in the absence of a textile flap. As can be seen from the figure, the values of Nu measured from the experiments are about 8% less than that calculated from the Gnielinski correlation [29, 30].

Results and discussion

In this section, the effects of flap shape and size on heat transfer performance are discussed prior to shifting focus to rectangular flaps, which were shown to provide superior convective heat transfer performance for the majority of the test conditions. In the second part of this section, the relationship between the heat transfer performance and the oscillating frequency of the rectangular flaps is explored.

Heat transfer in the presence of textile flaps

Figure 6 shows the plot of the air-side h varying with U in the absence of textile flaps and in the presence of flexible textile flaps of different shapes. It should be noted that all textile flaps shown in the figure have the same area. As can be seen from Figure 6, for all shapes of textile flaps, h increases monotonically as U increases. However, the h values and the rates of change of h with U vary from one textile shape to another. When U = 9.9 m/s (the lowest air velocity reported in this study), the h value for each shape of textile flap has a small deviation from that observed in the absence of textile flaps, indicating that the influence of the flexible textile flaps on h at a low air velocity is negligible. At the highest air velocity (U = 18.5 m/s), the h value for the inverted isosceles triangular shape is 158 W·m⁻² K⁻¹ which is nearly 40% higher than that for the case without a textile flap which is 118 W·m⁻²·K⁻¹. It is also observed that the performance of the isosceles triangular flap is lower than the baseline without flap at low velocities (i.e., $9.9 - 12.1 \,\mathrm{m/s}$). It is thought that the low air velocities present were unable to drive this shape flap into a fluttering motion state. This results in a predominantly stationary flap that rests on and insulates the hot plate, increasing the plate temperature over the baseline.

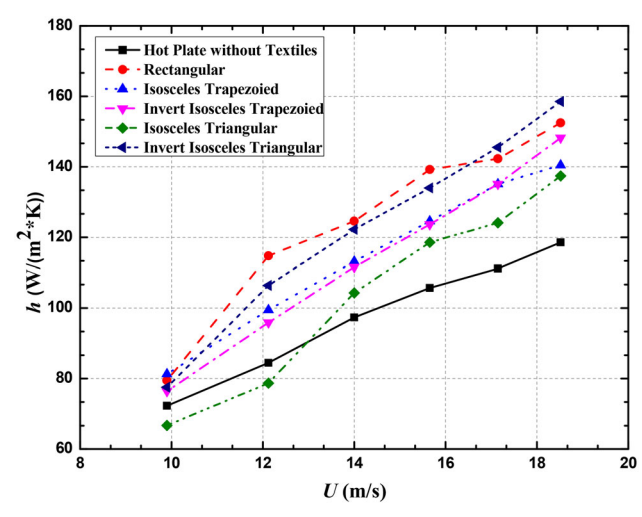
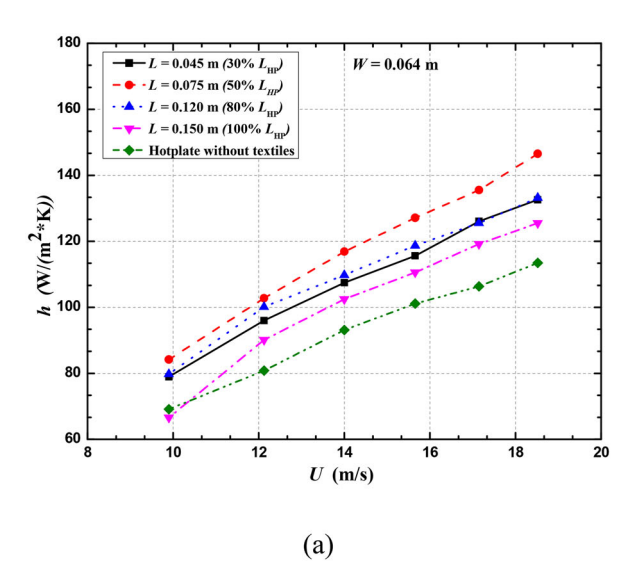
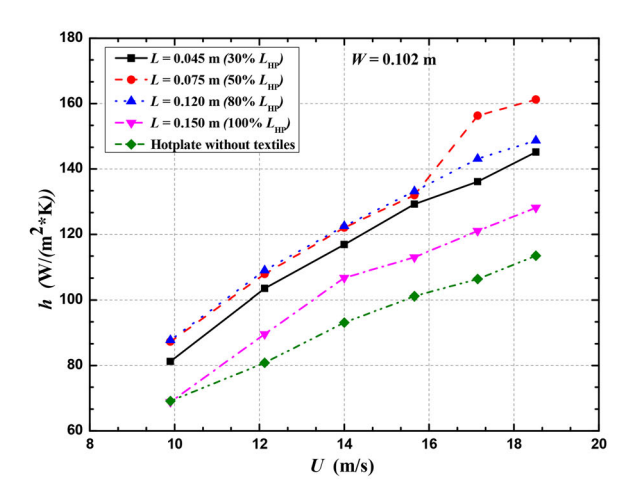


Figure 6. Heat transfer coefficient h vs. air velocity U for the textile flaps with different shapes but the same area.

In the range of wind velocities between 12.1 and 15.7 m/s, the rectangular flaps consistently outperformed the other shapes studied with h values ranging from $115 \,\mathrm{W \cdot m^{-2} \cdot K^{-1}}$ to $140 \,\mathrm{W \cdot m^{-2} \cdot K^{-1}}$. However, for air velocities greater than 17.1 m/s, the h value of the rectangular textile flap is slightly lower than that of the inverted isosceles triangular shape. This is likely caused by the change of the flutter mode of the rectangular textile flaps at high wind speeds [31], thus resulting in weaker flow mixing in the top portion of the hot plate and a slower rate of increase of h. In contrast, more vigorous three-dimensional motions of the inverted isosceles triangular textile flap at high wind speeds would strengthen the turbulence within the boundary layer near the hot plate surface and slightly increase the rate of change of h.

As shown in the previous section, the rectangular textile flap produced higher heat transfer enhancement in the range of wind velocities U between 12.1 and 15.7 m/s, compared to the other four flap shapes. Given this result, rectangular textile flaps were chosen to investigate the effects of textile flap dimensions on heat transfer and the relationship between the oscillatory motion and heat transfer. Twelve rectangular flaps comprised of four different lengths (0.045 m, 0.075 m, 0.120 m and 0.150 m) and three different widths (0.064 m, 0.102 m, and 0.127 m) were tested, and their heat transfer results are shown in Figure 7, where the four flap lengths are given as percentage of the hot plate length ($L_{\rm HP}=0.150\,{\rm m}$). As can be seen from Figure 7, h increases as U increases for all rectangular textile flaps. However, for a given width of the rectangular textile flap, the h values vary from one textile flap length to another. Also, for a given length of rectangular textile flap, h values vary from one





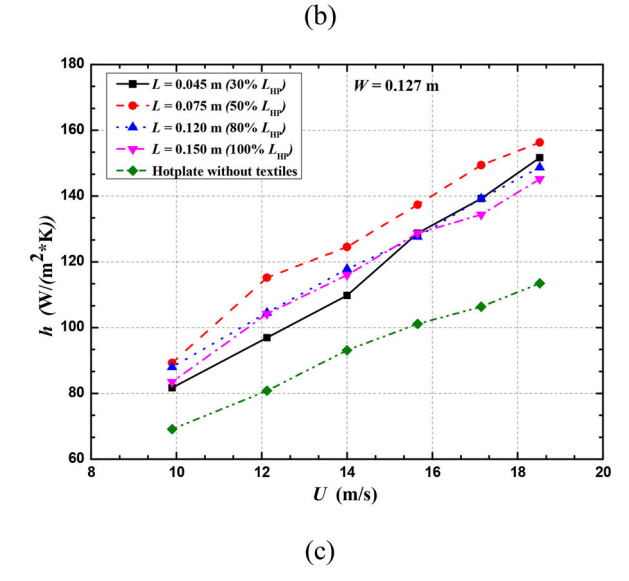


Figure 7. Heat transfer coefficient h vs. inlet air velocity U for different rectangular flap lengths L and widths W. The four flap lengths of 0.045 m, 0.075 m, 0.120 m and 0.150 m are labeled as 30% $L_{\rm HP}$, 50% $L_{\rm HP}$, 80% $L_{\rm HP}$, and 100% $L_{\rm HP}$, respectively. Here $L_{\rm HP}=0.150\,{\rm m}$ is the hot plate length. (a): $W=0.064\,{\rm m}$, (b): $W=0.102\,{\rm m}$, (c): $W=0.127\,{\rm m}$.



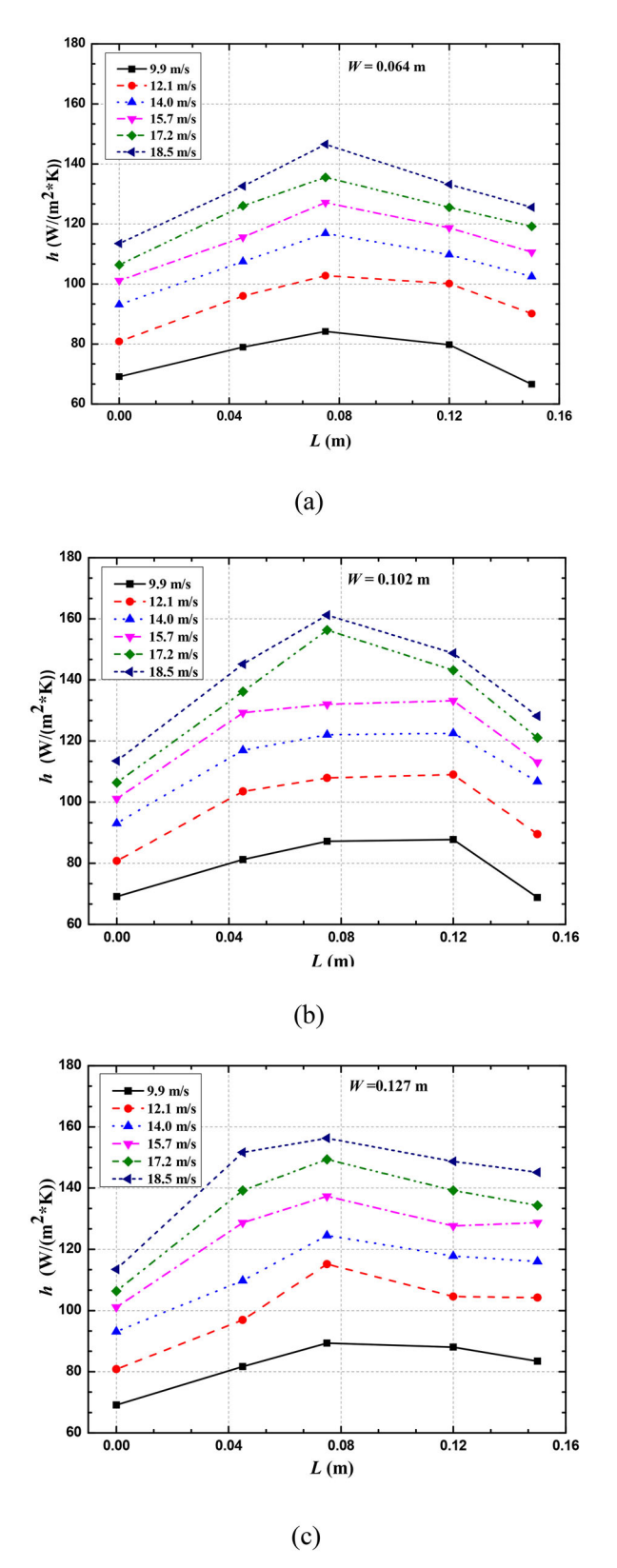


Figure 8. Heat transfer coefficient h vs. rectangular flap length L for different air velocities and flap widths W. The heat transfer coefficient h at 18.5 m/s in each subplot reaches a maximum at L = 0.075 m, which is about 50% of the hot plate length. (a): $W = 0.064 \,\text{m}$, (b): $W = 0.102 \,\text{m}$, (c): $W = 0.127 \,\text{m}$.

textile flap width to another. For instance, for the 0.064 m wide by 0.045 m long flap, the enhancement of h is about 67% from U = 9.9 to 18.5m/s, as illustrated in Figure 7(a), while for the textile flap of $0.127 \,\mathrm{m}$ wide by $0.045 \,\mathrm{m}$ long, the enhancement of his 86% from U = 9.9 to 18.5m/s, as shown in Figure 7(c). Figure 7 also shows that the textile flaps with a length of 0.075 m, (50% L_{HP}), are more effective at enhancing the heat transfer coefficient, compared to other flap lengths. To provide further illustration, the data in Figure 7 are replotted in Figure 8, where the heat transfer coefficient h is plotted against the flap length L for different airflow velocities and different flap widths W. It is interesting to note that the heat transfer coefficient h increases up to 50% of the length of the hot plate before gradually decreasing with any additional flap length. Maximum increase in heat transfer coefficient over the baseline is obtained for the 0.102m wide by 0.075m long flap at U = 18.5m/s where a 42% increase in h is observed. The heat transfer enhancement with this dimension of rectangular textile is likely related to the change of the flutter mode with the length change of the textile flap [31]. The observed optimal length (50% L_{HP}) of the rectangular flaps which maximizes the heat transfer coefficient, could be attributed to the superimposed adverse effects of lower oscillating frequency and beneficial effects of larger coverage area of flaps as their length increases. It is also observed in Figure 8(c) that the heat transfer coefficient for the air velocities of U = 12.1 and 15.7 m/s and the flap length L = 0.14 m is slightly higher than for $L = 0.12 \,\mathrm{m}$, which produces opposing trends, compared to other air velocities. Future research on the air velocity field near the hot plate is needed to explain this phenomenon. Overall, the size and shape of the textile flaps play an important role in the enhancement of heat transfer as these geometrical features dominate the flow-induced motion of the textile flap in the wind tunnel, which will be discussed further in the following section.

Oscillating frequencies of the rectangular textile flaps

Figure 9 shows six photographs of the free end of the rectangular flap captured with high speed camera at a wind speed of U = 18.5 m/s. These six images correspond to the six time-instances in a typical cycle of the oscillation of the textile flap. In the figure, the air flows downward, and the textile flap is 0.075 m long (50% of the hot plate length) by 0.102 m wide (80% of the hot plate width). The motion of the textile flap is

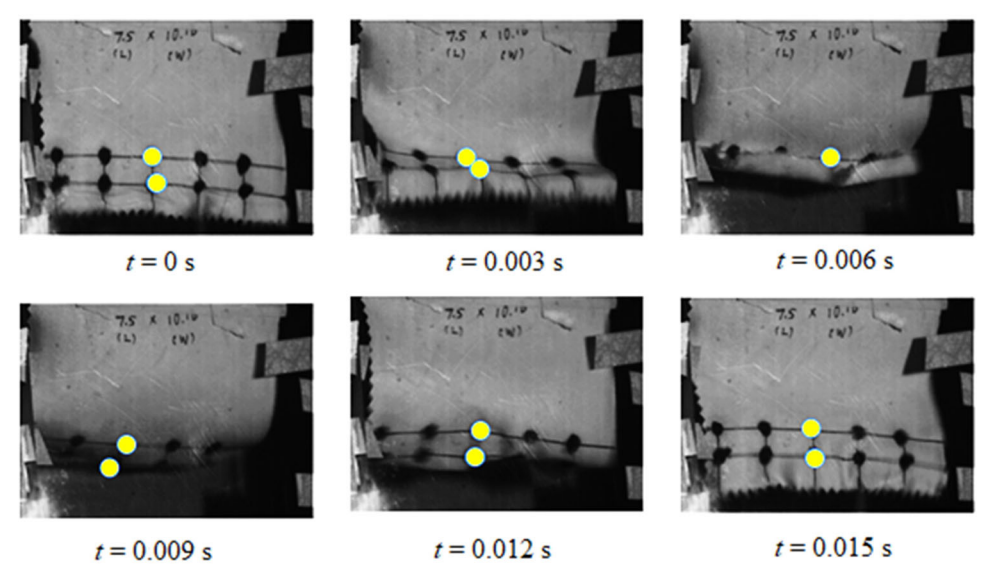


Figure 9. Images showing the oscillating motion of the rectangular textile flap of dimension $L \times W : 0.075 \text{m} \times 0.102 \text{ m}$. The time difference between the first and last images, referred to as the oscillating period, is 0.015 s, corresponding to an oscillating frequency of 66.67 Hz.

illustrated by the displacement of the dots and meshes marked on the flap. As can be seen from Figure 9, the flap primarily oscillates along the air-flow direction, though the free end of the flap does sometimes curl on itself. It should be noted that the amplitude of this oscillation has little variation with wind speed [31] and as such, the oscillating frequency of the flap is the critical parameter describing the oscillation dynamics. The time taken for the yellow dots seen in Figure 9 to cycle from their lowest positions back to those same positions is considered as one oscillation period, whose inverse is the oscillation frequency. The accuracy of the oscillation period measurement depends on the quality of the image and the wind speed. For the well-focused images typical of this study, the start and end of each period can be determined within two frames (2 ms in time) for high wind conditions, which corresponds to an uncertainty of about 5% in the frequency measurement.

Figure 10 shows the oscillating frequencies (f) of rectangular textile flaps varying with U. In this figure, the oscillating frequencies range from about 15.4 to 76.9 Hz, with corresponding oscillating periods measured to be between 0.013 to 0.065 seconds. As can be seen from Figure 10, oscillation frequency increases monotonically with wind speed for all rectangular textile flaps. This trend is similar to that reported by Virot et al. [31] who experimentally studied the dynamics of fluttering flags. As seen in Figure 10, the frequency values and the rates of change of oscillating frequency with increasing air velocity change from one flap dimension to another. For a given width, as

seen in Figure 10(a), the curve of f vs. U for $L = 0.045 \,\mathrm{m}$ is above that for $L = 0.075 \,\mathrm{m}$, indicating that the oscillating frequency of the rectangular textile flap decreases as the flap length increases. However, the vertical separation between these two curves becomes smaller when the width of the textile flaps increases from 0.064 m to 0.127 m. It is also reported by Teneda [32] that the oscillating frequencies of flags in a uniform flow increases with increasing mass per unit area of flags.

To explore the physical mechanisms that control the oscillation of textile flaps in the wind tunnel, we introduce two parameters: the area coverage ratio (A*) and dimensionless flow-induced oscillating frequency (f^*) . The area coverage ratio A^* is defined as the textile flap area over the hot plate area (A) as given below:

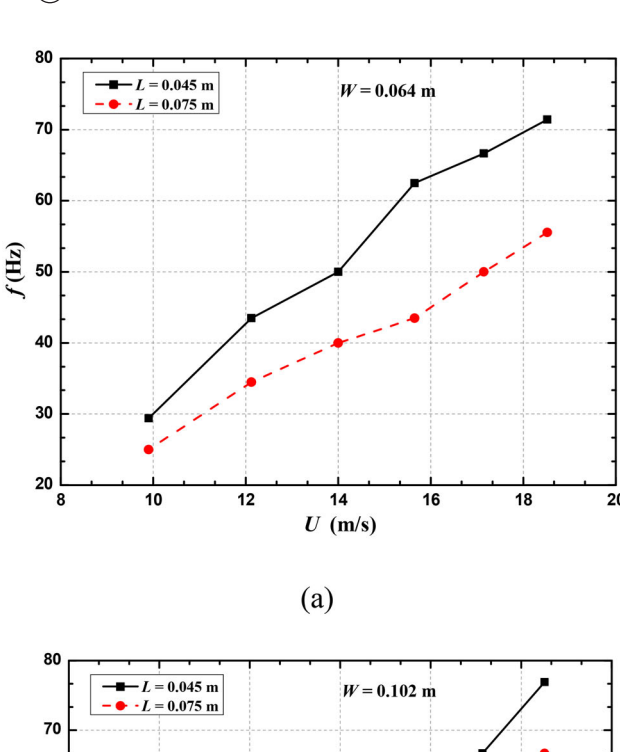
$$A^* = \frac{LW}{A} \tag{9}$$

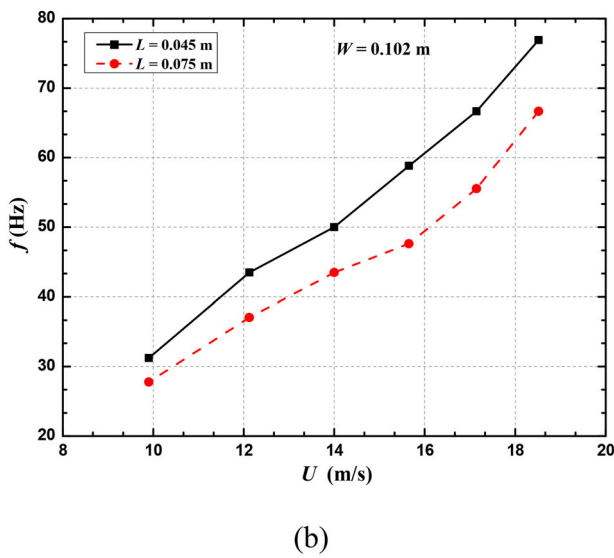
L and W are the length and width of the textile flap, respectively. The dimensionless oscillating frequency f^* representing the flow unsteadiness is defined as

$$f^* = \frac{fL}{U} \tag{10}$$

where f is the oscillating frequency of the flexible textile flap.

Figure 11 shows f^* as a function of A^* under different wind conditions. In the figure, the trend lines are polynomial fitting curves for different wind speeds. As can be seen from this figure, f^* increases with A^* , indicating that the flow unsteadiness





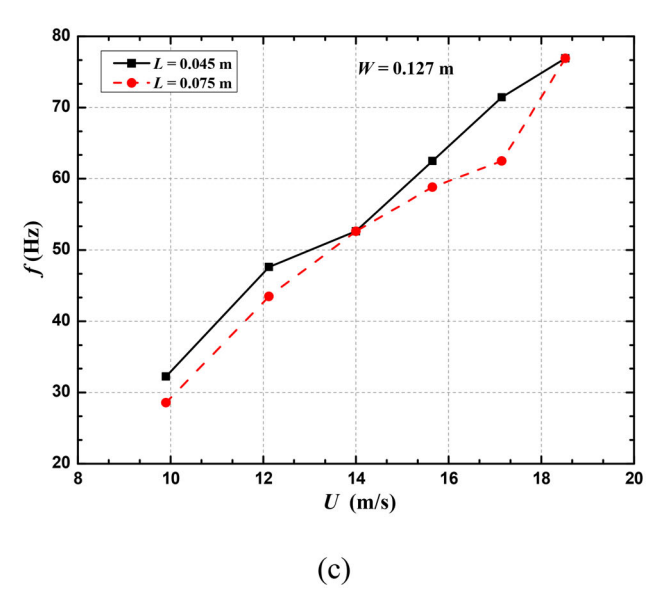


Figure 10. Oscillating frequency f vs. air velocity U for two rectangular flap lengths L and three widths W. (a): $W = 0.064 \,\text{m}$, (b): $W = 0.102 \,\text{m}$, (c): $W = 0.127 \,\text{m}$.

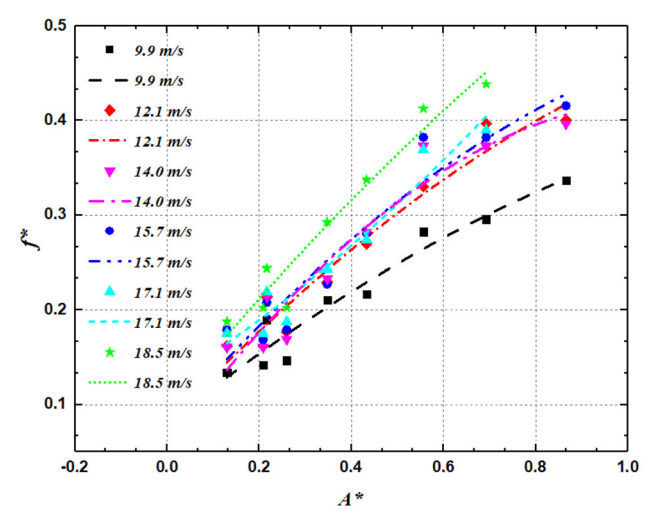


Figure 11. Dimensionless flow-induced oscillation frequency f^* vs. rectangular flap area coverage ratio A^* for different airflow velocities.

increases with increasing A^* . Figure 11 also shows that for a given A^* , f^* increases as the air flow velocity increases, indicating that f^* might be affected by Re. A plot of f^* versus a dimensionless parameter A^*Re is shown in Figure 12. As can be seen in the figure, the data points collapse to a single curve and f^* increases with increasing A^*Re in a nonlinear fashion. Using a curve fit to the data yields

$$f^* = 8.987 \times 10^{-4} (A^* Re)^{0.57} \tag{11}$$

with the coefficient of determination $R^2 = 0.912$. Eq. (11) reveals that the effects of the area coverage ratio A^* and Reynolds number Re are of equal importance in determining the dimensionless oscillating frequency f^* .

Correlation between the heat transfer coefficient and the oscillatory frequency of the textile flaps

As shown in the Experimental Uncertainty and Validation of Test Apparatus section, the present baseline experimental data set (hot plate without flap) fits the Gnielinski correlation [29, 30] for internal turbulent channel flow, as seen in Figure 5. For the sake of simplicity, the Gnielinski correlation shown in Eq. (7) may be altered to a more compact form as follows:

$$Nu = K(Re - 1000)$$
 (12)

where K is a heat transfer coefficient that represents the combined effects of f_D , $\frac{D_H}{L}$ and Pr. Figures 6 and 7 showed that the trend of heat transfer coefficient h with air velocity U in the absence of flaps is similar to the same trends in the presence of rectangular flaps. Similarly, a correlation such as Eq. (12) is able to fit the experimental data in the presence of flaps by

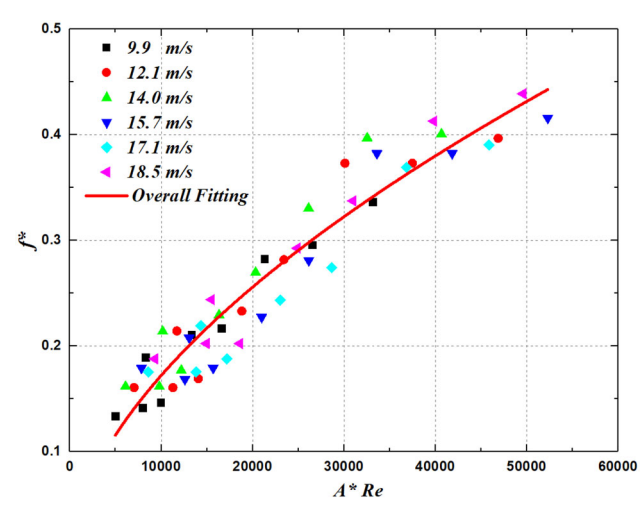


Figure 12. Dimensionless flow-induced frequency f^* varying with dimensionless parameter A^*Re for various air velocities. The solid line is the fitting curve: $f^* = 8.987 \times 10^{-4} (A^*Re)^{0.57}$ with the coefficient of determination $R^2 = 0.912$.

modifying the coefficient K appropriately. In this study, while the Prandtl number Pr is a constant, the friction factor f_D is changed by the enhancement of the flow mixing in the air boundary layer in the presence of the textile flap. However, f_D values are difficult to obtain due to the complexity of the textile flap oscillation in the air flow. Also, the effects of the thermal entry length $\frac{D_H}{L}$ become complicated in the presence of the flaps. In addition, it should be kept in mind that K also varies with Re because f_D is a function of Re, as indicated in Eq. (8). Given these results, the following explores the hypothesis that K is also correlated with the oscillating frequency of the textile flap.

Figure 13 shows the empirical relationship between the coefficient K = Nu/(Re-1000) and f^* . In the figure, the trend lines are fitted polynomial curves for various wind speeds, corresponding to different Re. As can be seen from Figure 13, for each airflow speed, K varies with f^* in a nonlinear fashion. In general, the maximum value of K occurs when f^* falls in the narrow range between 0.22 and 0.32, and this maximum varies with Re, ranged from 8×10^4 to 1.6×10^5 . Based on Eq. (12), Nu would also reach its maximum for its Re when f^* is between 0.22 and 0.32, which implies optimal heat transfer performance.

Such results might eventually be applied to the optimal design of future heat exchangers. For instance, for a heat exchanger with self-sustained oscillating textile flaps, we can first calculate the corresponding Re after U is determined. Then, to maximize the heat transfer performance, the optimal A^* describing the area coverage ratio between the textile flap and hot plate can be estimated with the calculated Re,

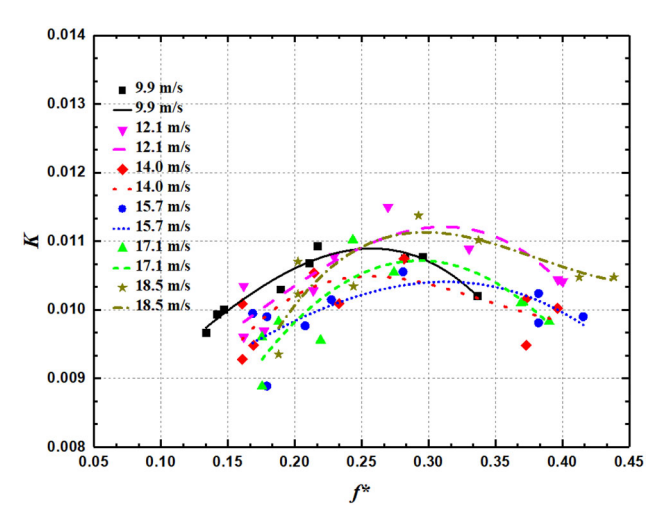


Figure 13. Coefficient K vs. dimensionless flow-induced oscillation frequency f^* for various air velocities.

based on Eq. (11) and Figure 13. In other words, the highest Nu may be achieved by optimizing the size of the textile flap to reach a certain value of f^* in the range of 0.22 to 0.32, depending on Re.

Conclusions

The present study investigated heat transfer enhancement on a flat plate with a flow-induced oscillating-slapping flexible textile flap where self-sustained periodic slapping of the heat transfer surface disrupts the boundary layers and thus enhances heat transfer between the air and the plate surface. The heat transfer coefficient of the plate was measured for textile flaps with different shapes and sizes and the motion of the textile flaps was captured using a high-speed camera. The main conclusions given the subsequent analysis are summarized as follows:

- 1. Heat transfer enhancement changes markedly with the shape and size of the textile flap depending on the wind speed. Among the shapes of textile flaps that were tested, rectangular textile flaps provided the largest enhancement of convective heat transfer for wind speeds less than 17.2 m/s where a maximum increase of about 42% in h was observed.
- Investigation into variables influencing the oscillating frequencies of rectangular flaps shows that air velocity and size of the textile flaps both play significant roles.
- 3. Expressing heat transfer performance by K = Nu/(Re-1000) and plotting against f^* indicates that maximum heat transfer performance occurs at a particular value of f^* in the range of 0.22 to 0.32, depending on the Reynolds number.

4. Correspondingly, an optimal design for future heat exchangers can be achieved by optimizing A^* for a given Re to reach a desired f^* in the range of 0.22 to 0.32 based on Eq. (11) and Figure 13.

Acknowledgement

B. Yang acknowledges the support of the National Science Foundation (NSF) under the award number 1706777.

Notes on contributors



Beihan Zhao is a Ph.D. student in the Department of Mechanical Engineering at the University of Maryland, College Park, USA. He received his B.Eng. in Mechanical Design, Manufacture and Automation in University of Electronic Science and Technology of China in 2016. His research interests are in heat transfer,

advanced manufacturing, and electronic packaging.



Wenshuo Yang is a visiting graduate student at University of Maryland, College Park, USA. She got a B.S. degree from Xian Jiao Tong University in China in 2013. Her research interests are in both the experimental and numerical analysis based on film cooling method on cascades of gas turbine and optimization of cooling

method using heat sink.



Chaolun Zheng is a Ph.D. student and research assistant in the Department of Mechanical Engineering at the University of Maryland, College Park, USA. He received his B.S. in Chemistry from the University of Science and Technology of China in 2014. His research interests are in high efficiency cooling system, advanced

absorbent and thermal fluids, nanomaterials for energy storage, and simulation using finite element methods.



Yong Pei is a Ph.D. student in the Department of Mechanical Engineering at the University of Maryland, College Park, USA. He received a Master's Degree in Power Engineering and Engineering Thermo-physics from Xi'an Jiaotong University in 2017. His research interests are in heat transfer and thermal property

measurement.



Anthony Malatesta is a Ph.D. student in the Department of Mechanical Engineering at the University of Maryland, College Park, USA and the founder and team lead of NAVAIR's Thermal and Electrical Modeling Lab at NAS Patuxent River, MD. His research interests are in thermal management and fluid thermo-

physical property modeling.



Xinan Liu is a Research Professor in the Department of Mechanical Engineering at the University of Maryland, College Park, USA. He received his Ph.D. from the same university in 2002 His research interests are in experimental and theoretical/numerical investigations of fluid flows and fluid-structure interactions.



Bao Yang is a Professor in the Department of Mechanical Engineering at the University of Maryland, College Park, USA and currently directs the Micro/Nanoscale Heat Transfer and Energy Conversion Laboratory. He received his Ph.D. from University of California, Los Angles, USA in 2003. His research inter-

ests are in thermal management, micro/nanoscale thermal transport and energy conversion, and advanced materials for thermal management and energy conversion.

References

- [1] S. Liu and M. Sakr, "A comprehensive review on passive heat transfer enhancements in pipe exchangers," *Renew. Sustain. Energy Rev.*, vol. 19, no. 3, pp. 64–81, 2013. DOI: 10.1016/j.rser.2012.11.021.
- [2] O. Yemenici and H. Umur, "Experimental aspects of heat transfer enhancement over various flow surfaces," *Heat Transfer Eng.*, vol. 37, no. 5, pp. 435–442, 2016. DOI: 10.1080/01457632.2015.1057449.
- [3] S. Kakaç and A. Pramuanjaroenkij, "Review of convective heat transfer enhancement with nanofluids," *Int. J. Heat Mass Transfer*, vol. 52, no. 13-14, pp. 3187–3196, 2009. DOI: 10.1016/j.ijheatmasstransfer. 2009.02.006.
- [4] G. Li, Y. Zheng, G. Hu, Z. Zhang and Y. Xu, "Experimental study of the heat transfer enhancement from a circular cylinder in laminar pulsating cross-flows," *Heat Transfer Eng.*, vol. 37, no. 6, pp. 535–544, 2016. DOI: 10.1080/01457632.2015.1060758.
- [5] E. I. Nesis, A. F. Shatalov and N. P. Karmatskii, "Dependence of the heat transfer coefficient on the vibration amplitude and frequency of a vertical thin heater," *J. Eng. Phys. Thermophys.*, vol. 67, no. 1-2, pp. 696–698, 1995. DOI: 10.1007/BF00853316.
- [6] A. Suksangpanomrung, S. Chungpaibulpatana and P. Promvonge, "Numerical investigation of heat transfer in pulsating flows through a bluff plate," *Int.*



- Commun. Heat Mass Transfer, vol. 34, no. 7, pp. 829-837, 2007. DOI: 10.1016/j.icheatmasstransfer. 2007.03.013.
- J. Wajs, D. Mikielewicz, E. Fornalik-Wajs and M. Bajor, "High performance tubular heat exchanger with minijet heat transfer enhancement," Heat Transfer Eng., vol. 40, no. 9-10, pp. 772-783, 2019. DOI: 10.1080/01457632.2018.1442369.
- P. Wang, et al., "Sweating-boosted air cooling using nanoscale CuO wick structures," Int. I. Heat Mass Transfer, vol. 111, no. 8, pp. 817-826, 2017. DOI: 10. 1016/j.ijheatmasstransfer.2017.04.042.
- C.-C. Wang, "A survey of recent patents of fin-andtube heat exchangers from 2001 to 2009," Int. J. Air-Cond. Ref., vol. 18, no. 01, pp. 1-13, 2010. DOI: 10. 1142/S2010132510000022.
- [10] C.-C. Wang, K.-Y. Chen, J.-S. Liaw and C.-Y. Tseng, "An experimental study of the air-side performance of fin-and-tube heat exchangers having plain, louver, and semi-dimple vortex generator configuration," Int. J. Heat Mass Transfer, vol. 80, no. 1, pp. 281–287, 2015. DOI: 10.1016/j.ijheatmasstransfer.2014.09.030.
- [11] M. Sheikholeslami, M. Gorji-Bandpy and D. D. Ganji, "Review of heat transfer enhancement methods: Focus on passive methods using swirl flow devices," Renew. Sustain. Energy Rev., vol. 49, no. 9, pp. 444-469, 2015. DOI: 10.1016/j.rser.2015.04.113.
- Varun, M. O. Garg, H. Nautiyal, S. Khurana and M. K. Shukla, "Heat transfer augmentation using twisted tape inserts: A review," Renew. Sustain. Energy Rev., vol. 63, no. 9, pp. 193-225, 2016. DOI: 10.1016/j.rser.2016.04.051.
- [13] D. Gerty, "Fluidic-driven cooling of electronic hardware: part I: channel integrated vibrating reed part II: active heat sink," PhD dissertation, School of Mechanical Engineering, Georgia Institute of Technology, 2008.
- [14] P. Hidalgo, F. Herrault, A. Glezer, M. Allen, Ed., "Heat Transfer Enhancement in High-Power Heat Sinks using Active Reed Technology," presented at 2010 16th International Workshop on Thermal Investigations of ICs and Systems (THERMINIC), Barcelona, Spain, Oct. 6-8, 2010.
- K. Shoele and R. Mittal, "Computational study of flow-[15] induced vibration of a reed in a channel and effect on convective heat transfer," Phys. Fluids, vol. 26, no. 12, pp. 127103-127124, 2014. DOI: 10.1063/1.4903793.
- T. Açı kalı n, S. M. Wait, S. V. Garimella and A. [16] Raman, "Experimental investigation of the thermal performance of piezoelectric fans," Heat Transfer Eng., vol. 25, no. 1, pp. 4–14, 2004. DOI: 10.1080/ 01457630490248223.
- [17] T. Açı kalı n, S. V. Garimella, A. Raman and J. Petroski, "Characterization and optimization of the thermal performance of miniature piezoelectric fans," Int. J. Heat Fluid Flow, vol. 28, no. 4, pp. 806-820, 2007. DOI: 10.1016/j.ijheatfluidflow.2006.10.003.
- S. M. Wait, S. Basak, S. V. Garimella and A. Raman, "Piezoelectric fans using higher flexural modes for electronics cooling applications," IEEE Trans. Comp. Packag. Technol., vol. 30, no. 1, pp. 119-128, 2007. DOI: 10.1109/TCAPT.2007.892084.

- Z. Li, et al., "Airfoil-shaped self-agitator for convective heat transfer enhancement," Int. J. Thermal Sci., vol. 133, pp. 284–298, 2018. DOI: 10.1016/j.ijthermalsci.2018.07.038.
- [20] K. Li, S. Wang, Z. Ke and C.-L. Chen, "A novel caudalfin-inspired hourglass-shaped self-agitator for air-side heat transfer enhancement in plate-fin heat exchanger," Energy Convers. Manage., vol. 187, no. 5, pp. 297-315, 2019. DOI: 10.1016/j.enconman.2019.03.048.
- K. Li, et al., "Air-side heat transfer enhancement in [21] plate-fin channel with an airfoil-based self-agitator," Int. J. Heat Mass Transfer, vol. 128, no. 1, pp. 715–727, 2019. DOI: 10.1016/j.ijheatmasstransfer. 2018.09.040.
- S. Wang, K. Li, Z. Ke and C.-L. Chen, "Time-[22] resolved PIV measurement and thermal-hydraulic performance evaluation of thin film self-agitators in a rectangular channel flow," Int. J. Heat Mass Transfer, vol. 137, no. 7, pp. 922-939, 2019. DOI: 10. 1016/j.ijheatmasstransfer.2019.04.014.
- S. Ali, C. Habchi, S. Menanteau, T. Lemenand and J.-L. Harion, "Heat transfer and mixing enhancement by free elastic flaps oscillation," Int. J. Heat Mass Transfer, vol. 85, no. 6, pp. 250-264, 2015. DOI: 10. 1016/j.ijheatmasstransfer.2015.01.122.
- S. Ali, S. Menanteau, C. Habchi, T. Lemenand and J.-L. [24] Harion, "Heat transfer and mixing enhancement by using multiple freely oscillating flexible vortex generators," Appl. Thermal Eng., vol. 105, no. 7, pp. 276-289, 2016. DOI: 10.1016/j.applthermaleng.2016.04.130.
- J. B. Lee, S. G. Park, B. Kim, J. Ryu and H. J. Sung, [25] "Heat transfer enhancement by flexible flags clamped vertically in a Poiseuille channel flow," Int. J. Heat Mass Transfer, vol. 107, no. 4, pp. 391-402, 2017. DOI: 10.1016/j.ijheatmasstransfer.2016.11.057.
- [26] J. B. Lee, S. G. Park and H. J. Sung, "Heat transfer enhancement by asymmetrically clamped flexible flags in a channel flow," Int. J. Heat Mass Transfer, vol. 116, no. 1, pp. 1003–1015, 2018. DOI: 10.1016/j. ijheatmasstransfer.2017.09.094.
- A. K. Soti, R. Bhardwaj and J. Sheridan, "Flow-[27] induced deformation of a flexible thin structure as manifestation of heat transfer enhancement," Int. J. Heat Mass Transfer, vol. 84, no. 5, pp. 1070-1081, 2015. DOI: 10.1016/j.ijheatmasstransfer.2015.01.048.
- R. J. Moffat, "Describing the uncertainties in experi-[28] mental results," Exp. Thermal Fluid sci., vol. 1, no. 1, pp. 3-17, 1988. DOI: 10.1016/0894-1777(88)90043-X.
- [29] V. Gnielinski, "New equations for heat and mass transfer in the turbulent flow in pipes and channels," NASA STI/Recon Tech. Rep. A, vol. 41, no. 1, pp. 8–16, 1975.
- [30] N. Coetzee, "Heat transfer coefficients of smooth tubes in the turbulent flow regime," MEng dissertation, Dept. Mech. and Aero. Eng., University of Pretoria, Pretoria, South Africa, 2015.
- E. Virot, X. Amandolese and P. Hémon, "Fluttering [31] flags: An experimental study of fluid forces," J. Fluids Struct., vol. 43, no. 11, pp. 385-401, 2013. DOI: 10.1016/j.jfluidstructs.2013.09.012.
- S. Taneda, "Waving motions of flags," J. Phys. Soc. [32] Jpn., vol. 24, no. 2, pp. 392-401, 1968. DOI: 10.1143/ JPSJ.24.392.